Unified constitutive equations to describe elastoplastic and damage behavior of an X100 linepipe steel

Thanh Trung Luu, Benoit Tanguy, Jacques Besson, André Pineau, G. Perrin

UNIFIED CONSTITUTIVE EQUATIONS TO DESCRIBE ELASTOPLASTIC AND DAMAGE BEHAVIOR OF AN X100 LINEPIPE STEEL

T.T Luu[*,**], B. Tanguy[*], J. Besson[*], A. Pineau[*], G. Perrin[**]
(*) École des Mines de Paris, Centre des Matériaux, UMR CNRS 7633,
91003 Évry Cedex, France
(**) Applied Mechanics Division, Institut Français du Pétrole, 92500 Rueil-Malmaison, France

E-mail: luu@mat.ensmp.fr, btanguy@mat.ensmp.fr

Abstract

The deformation and fracture of the high strength steel which is used to fabricate grade X100 steel pipe were investigated at room temperature, on plate and pipe. Anisotropic behaviour was characterized by using tensile tests conducted along different directions. The fracture toughness of plate and pipe materials are compared using compact tension (CT) and Charpy V-notched tests. In both cases, these materials give rise to good fracture properties. The aim of the present study is to establish unified constitutive equations able to describe the elastoplastic and damage behavior of one X100 linepipe steel. The model is then used to simulate three point bending and compact tension tests.

1. Introduction

Economic gas transportation over long distances requires high pressure and consequently high strength steels such as grade X100 (YS>690MPa) which is investigated in this study. Steel plate produced by Thermo-Mechanical Controlled Process (TMCP) is formed into large diameter pipe. Fracture propagation of these steels must be determined to assess the integrity of pipelines. Ductile crack propagation and crack arrest properties are based mainly on a Battelle two curves approach or on a CTOA model. These approaches have shown some limitations for high strength steels. An attempt is made to use the local approach to ductile fracture [1] to reduce these limitations. The robustness of this approach relies on a fine description of the involved fracture micro-mechanisms and of the stress-strain states. The purpose of this study is to establish unified constitutive equations able to represent both the plastic and rupture behavior of plate and pipe. The model must then account for plastic anisotropy (induced by the production process) and for the pre-strain effect resulting from forming plate into pipe.

2. Materials and experimental procedures

A plate with a nominal thickness of 18.4mm and a pipe ring of X100 steel pipe 36"x20mm were supplied by Europipe. Plate is elaborated using controlled rolling and accelerated cooling and then formed into a pipe using UOE process [2].The plate and the pipe will be referred as P and Pi, respectively. In the following, the rolling direction of the plate (before forming) is referred to as L, the long transverse direction as T and the short transverse direction (thickness) as S.

Both plate and pipe were examined by optical microscopy and scanning electron microscopy (SEM) after having been mechanically polished and etched in 4% nital solution.

The inclusions were observed and characterized using quantitative metallography. Two sections in planes L-S and T-S respectively, at half-thickness of the plate and the pipe**,** were analysed

using scanning electron microscopy. The inclusions were characterized using X-ray energy dispersive spectroscopy.

The anisotropy of deformation of the plate and the pipe was determined through a set of tension tests (TR) conducted along L, T and S directions. The smooth tensile (ST) specimens were 5mm diameter (in gauge) cylindrical bars for L, T directions and 3mm diameter (in gauge) for S direction (Fig. 1a). For each tensile test, the axial extension and diameter reduction along both the short transverse direction and the direction perpendicular to S were measured. An elongation strain rate $\dot{e} = 5.10^{-4} s^{-1}$ was used for all the tests.

Axisymmetrically notched tensile (NT) specimens were machined along the longitudinal and transverse directions for both plate and pipe. These specimens are defined by the ration R/Φ_0 where R is the radius of the notch and Φ_0 the minimum diameter. Three notch geometries were considered (NT_1, NT_2 and NT_4) (Fig. 1b). One diametral MTS extensometer was positioned in the minimal section of the notched bar along the short transverse direction. Diameter reduction of the minimum cross section was continuously measured during testing. Diameter reduction control was used in order to interrupt some of the test before final fracture. The samples were then broken at liquid nitrogen temperature to observe the fracture surfaces corresponding to different ductile crack propagation states.

Crack growth resistance of plate and pipe materials were investigated using CT-12.5 compact tension specimens. Two loading directions (L-T and T-L) were investigated (see figure 2). The $J - \Delta a$ resistance curve was determined using both unloading compliance method and multi-specimen technique in accordance with ASTM-E1820. With the single specimen technique, test specimens were side-grooved in order to avoid tunnelling and maintain a straight crack front and deeply pre-cracked (a/W = 0.63). A total thickness reduction 0.20 B was applied. With the multiple specimen technique, specimens without side grooves were loaded to various levels and then unloaded. The ductile crack extension Δa was determined from direct measurements of the crack surface of the specimens which were broken at liquid nitrogen temperature after unloading.

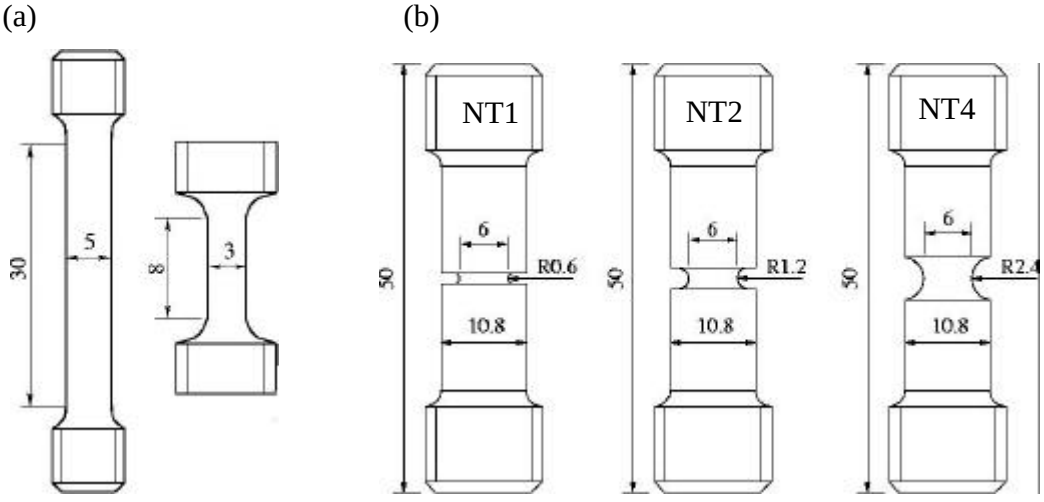

Figure 1: Tensile specimens for mechanical tests, (a) smooth tensile (b) axisymmetrically notched. Dimensions are in mm.

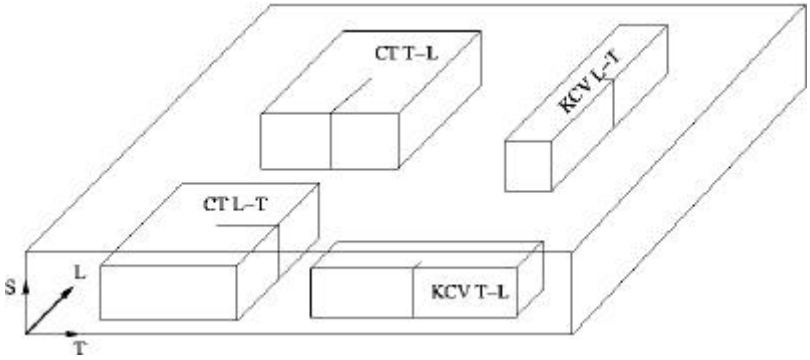

Figure 2: Shematic diagram showing CT and Charpy specimen orientations used in this study.

Standard Charpy V-notch (KCV) specimens along two loading directions (L-T et T-L, see figure 2) were tested in accordance with the standard (NF EN 10045-1) using an intrumented 450J capacity impact tester. In addition to these impact tests, three point-bend experiments were carried out on a servohydraulic machine at prescribed cross-head velocity of 10μm/s. A special set-up was designed to have the same contact conditions (hammer and anvils) as those for a conventional Charpy impact test.

3. Experimental results

Microstructure

The microstructure of grade X100 steel pipe (Pi) is shown in figure 3. It is constituted of acicular ferrite (zone A) and granular bainitic bands (zone B). Zone A is characterized by parallel groups of laths with an average length of approximately 4-5 μm. The size width of this zone is approximately 10μm. The main feature of zone B is the presence of equiaxed grains which have a fine substructure. The microstructure of the plate material is similar to that of the pipe, except that it is significantly finer and more homogeneous. In both materials, polished sections reveal the presence of inclusions which are major factors regarding damage tolerance. Most inclusions are composed of calcium sulphides or oxides. They are round shaped with a diameter of 2-5μm. The total volume fraction of inclusions has been estimated by image analysis using about 50 scanning electron micrographs at magnification 700 for each observed plane (L-S or T-S). For steel P, a value $f_i = 1.35 \times 10^{-4}$ was obtained.

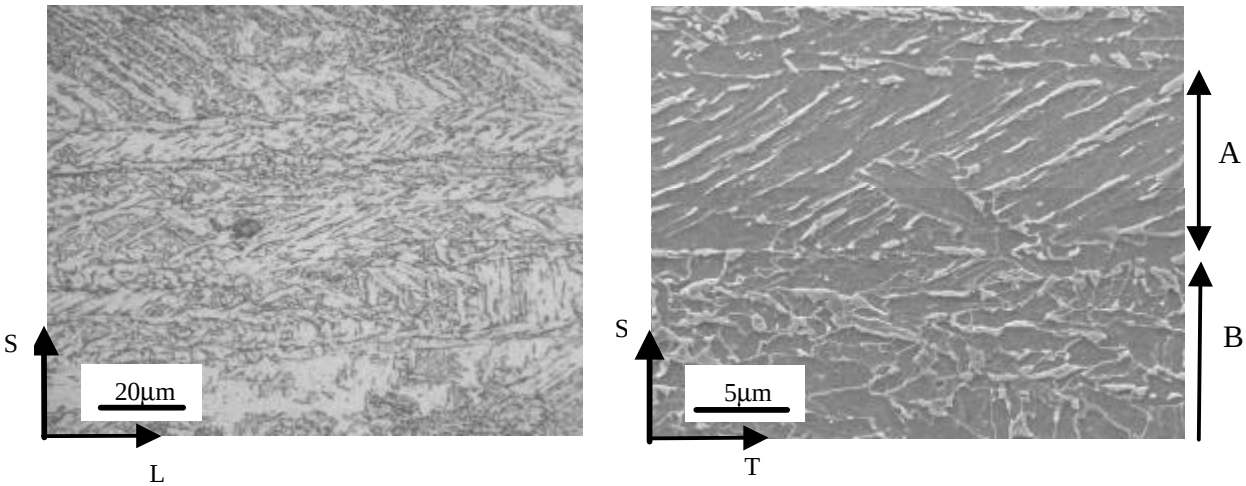

Figure 3: Steel ***Pi*** microstructure consisting of ferrite grains and bainite bands.

Anisotropy of deformation

Table 2 summarizes the mechanical properties (yield strength (YS), ultimate yield strength (UTS) and uniform elongation (UE)) of steels P and Pi along the principal directions: L, T and S. Because the pre-strain due to the plate to pipe process is not homogeneous in the pipe, the values of yield strength are more scattered for steel Pi (figure 4). Initially circular cross-sections of tensile specimens become elliptic upon deformation due to plastic anisotropy. The plastic anisotropy was characterized using Lankford coefficient R_I (I = L, T or S) where R_I is defined as the ratio of the reduction in diameter in two perpendicular directions. The Lankford coefficient is calculated under longitudinal loading as (e.g.):

$$R_L = \frac{e_T}{e_S} = \frac{\ln(F_T/F_0)}{\ln(F_S/F_0)} \quad (1)$$

where F_T, F_S are the current diameters along T and S. Note that $R_T = \varepsilon_S/\varepsilon_L$ so that a value of R_T (resp. R_L) greater (resp. smaller) than 1 reflects a higher deformability of the steels along the short transverse direction. The values reported in table 2 are those recorded after some sufficient axial strain (2-4%).

Evaluations of YS 0.2% and UTS as a function of the loading directions are given in figure 4 for plate and pipe. The X100 grade is obtained on the pipe ($YS_{(T)}$>690MPa) after UOE forming plate in pipe. In our case the plate showed a difference with the pipe in tensile properties knowing these materials are issued from a different heat.

Load direction I	Plate				Pipe			
	0.2% YS (MPa)	UTS (MPa)	UE (%)	R_I	0.2% YS (MPa)	UTS (MPa)	UE (%)	R_I
L	574	770	7.8	0.50	658	748	4.6	0.69
T	614	797	6.6	1.25	746	772	4.1	1.15
S	606	759	6.1	1.47	683	754	5.3	-

Table 2: X100 steel plate and pipe mechanical properties

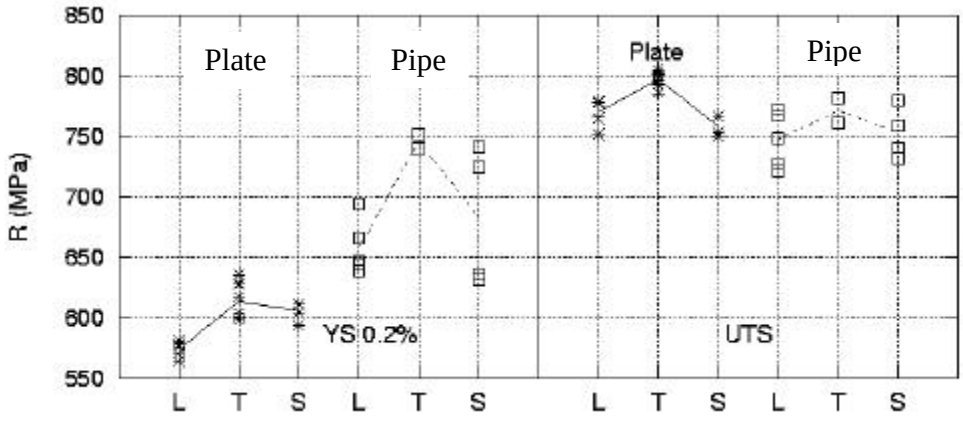

Figure 4: Yield strength at 0.2% plastic strain and ultimate tensile strength occurring from plate to pipe for three directions.

Notch sensitivity

The results of the tests on NT specimens of plate and pipe are reported in figure 5. For a given specimen geometry, the diameter reduction at crack initiation, along direction S, $\Delta\Phi_S^c$ is reported. These results show a large influence of notch geometry, hence stress triaxiality on the ductility at rupture which is calculated from the results of finite element calculations.

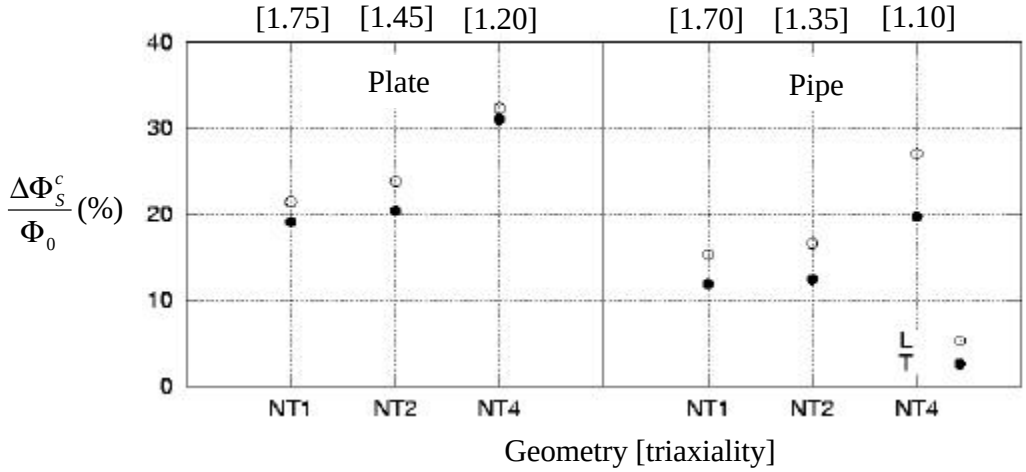

Figure 5: Diameter reduction at crack initiation in round notched bars.

Crack growth resistance

Evaluation of J values versus stable crack extension are shown in figure 6. A strong anisotropy behavior is observed on the J-Δa resistance curves where it is noted that in the plate $J_{02}^{LT} = 1.46 J_{02}^{TL}$ and in the tube $J_{02}^{LT} = 1.37 J_{02}^{TL}$. Lower fracture toughness properties are observed on pipe compared to plate material. Further work is under progress to see if this difference is related to the microstructure of the materials or to the forming process. Delaminations are observed for all tests excluded L-T configuration of pipe material.

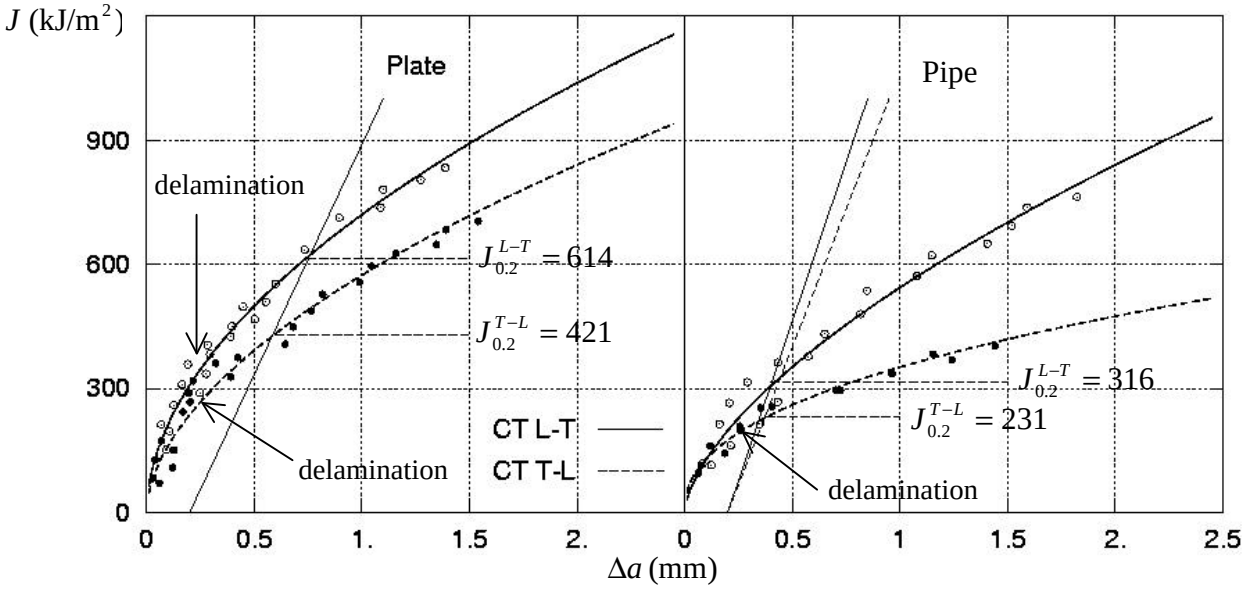

Figure 6: $J - \Delta a$ curves for the plate and the pipe.

Effect of impact velocity

Load-displacement curves issued from instrumented Charpy tests for the plate and for the pipe, for two configurations (L-T and T-L) are reported on figure 7. The maximum load is obtained for the pipe due to pre-strain. However, for the T-L solicitation a sharp drop of the load in the case of the pipe is observed once ductile crack propagation has initiated. This results in a strong decrease of the USE for the pipe. The USE for the plate and pipe at different impact velocites are given in table 3. The USE decreases when velocity decreases from 5m/s to 10µm/s. This behavior is mainly related to the increase in flow stress with strain rate. Delaminations are observed for T-L configuration of pipe material and for L-T configuration of plate material at 5m/s. At 10µm/s, delaminations are also observed for L-T solicitation of pipe material.

Loading direction	Plate		Pipe	
	5m/s	10µm/s	5m/s	10µm/s
L-T	296 J	237 J	277 J	211 J
T-L	309 J	234 J	237 J	178 J

Table 3: Charpy V-notch upper shelf energy for the plate and the ***pipe*** at different impact velocities (average values over 3 tests).

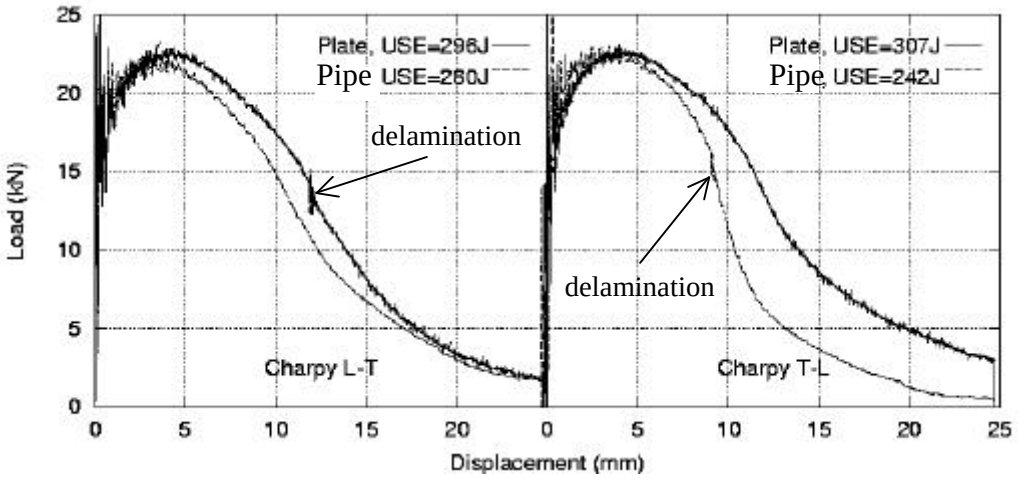

Figure 7: Load-displacement curves for the impact dynamic Charpy test for plate and pipe**.**

4. Material model

Elastoplastic behavior

As indicated above, the materials investigated present an anisotropic behavior which is not well represented by von Mises. As Hill criterion was not able to simulate accurately the anisotropic elastoplastic behavior, a particular case of the model proposed by Bron et Besson (2003) [3] was used. It is defined by an equivalent stress, $\bar{s}$, given by the following equations:

$$\bar{s} = \left(a\Psi^1 + (1-a)\Psi^2\right)^{1/a} \tag{2}$$

$$\Psi^1 = \frac{1}{2}\left(\left|S_2^1 - S_3^1\right|^a + \left|S_3^1 - S_1^1\right|^a + \left|S_1^1 - S_2^1\right|^a\right) \tag{3}$$

$$\Psi^2 = \frac{3^a}{2^a + 2}\left(\left|S_1^2\right|^a + \left|S_2^2\right|^a + \left|S_3^2\right|^a \right) \tag{4}$$

and for k = 1, 2, $S^k_{i=1,3}$ are the principal values of a modified stress deviator $\underline{s}^k$, k = 1, 2 defined as follows:

$$s^k_{11} = \frac{\left(c^k_2 + c^k_3\right)s_{11} - c^k_2 s_{22} - c^k_3 s_{33}}{3}, \quad s^k_{12} = c^k_4 s_{12}, \tag{5}$$

$$s^k_{22} = \frac{\left(c^k_3 + c^k_1\right)s_{22} - c^k_3 s_{33} - c^k_1 s_{11}}{3}, \quad s^k_{13} = c^k_5 s_{13}, \tag{6}$$

$$s^k_{33} = \frac{\left(c^k_1 + c^k_2\right)s_{33} - c^k_1 s_1 - c^k_2 s_{22}}{3}, \quad s^k_{23} = c^k_6 s_{23}. \tag{7}$$

Note that the classical Von Mises criterion is retrieved for α = 1, a = 2 and $c^{k=1,2}_{i=1,..,6} = 1$; Tresca criterion for α = 1, a = 8 and $c^{k=1,2}_{i=1,..,6} = 1$.

The yield surface is defined by :

$$f = \bar{s} - R(p) \tag{8}$$

where the flow stress of the material is expressed as a function of plastic strain, p, as:

$$R(p) = R_0\left[1 + Q_1\left(1 - e^{-k_1 p}\right) + Q_2\left(1 - e^{-k_2 p}\right)\right] \tag{9}$$

Parameters R_0, Q_1, Q_2, k_1, k_2 are all adjusted to fit the uniaxial tensile tests.

Use of this model requires the determination of several unknown material parameters related to hardening and anisotropic behaviour. The strategy to identification of these parameters was the same than the one used in [3]. They were adjusted from smooth tensile, notched tensile specimen testing and the Lankford coefficients.

The fitted values of model parameters obtained for the plate are presented in table 4. Figure 8 shows the comparisons between experiments, the anisotropic model and a von Mises criterion for the plate. It is shown that von Mises criterion is enable to simulate accurately the smooth tensile tests and overestimates the load of NT tests. A good agreement between experiments and calculations is obtained with the anisotropic model.

Moreover, considering a pre-strain of 2%, the constitutive equations well describe the behavior of notched specimens cut from the tube (see figure 8).

Damage

Ductile failure is commonly represented by models using a single damage parameter which represents the void volume fraction, or porosity, f. The Gurson model extended by Tvergaard and Needleman (so called GTN model) is used. The plastic flow potential, f, is written as:

(a)

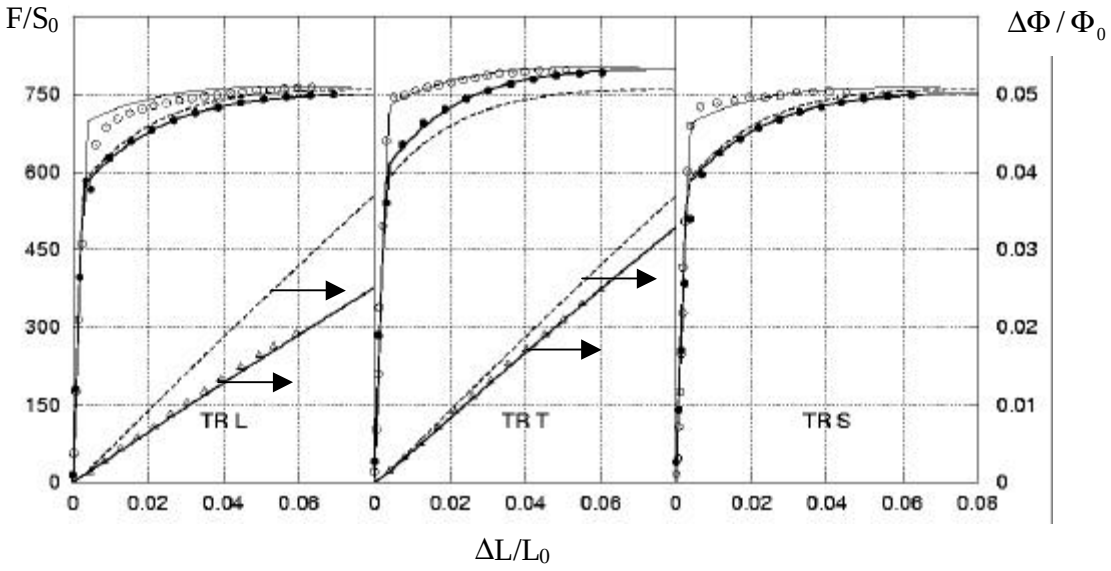

(b)

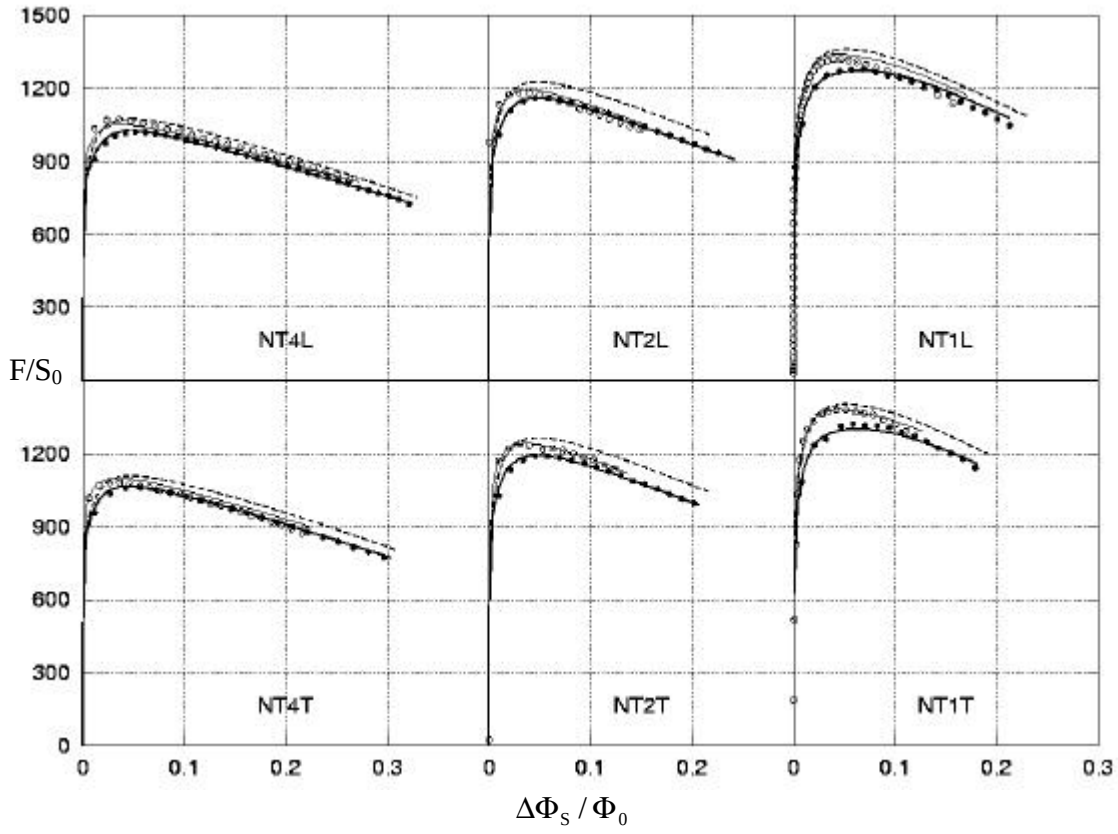

Figure 8: Comparison between experiments on plate (open symbols) and pipe (filled symbols), von Mises simulations (dashed lines) and simulations with the anisotropic model for the plate (solid lines) and for the pipe (thin solid lines). (a) smooth tensile, (b) axisymmetrically notched. F/S_0 is in MPa.

$$f = s_* - R(p) \tag{10}$$

The effective stress, s_*, is implicitly defined as:

$$\left(\frac{\bar{s}}{s_*}\right)^2 + 2q_1 f_* \cosh\left(\frac{3}{2} q_2 \frac{s_m}{s_*}\right) - 1 - q_1^2 f_*^2 = 0 \tag{11}$$

where $\bar{s}$ is the equivalent stress and s_m the mean stress, q_1 and q_2 are constant parameters ($q_1 = 1.5$ and $q_2 = 1$). f_* is an effective porosity. It is a function of the actual porosity f which has been introduced by Tvergaard and Needleman [4] to represent void coalescence leading to final fracture. It is expressed as:

$$f_* = \begin{cases} f & \text{if } f < f_c \\ f_c + d(f - f_c) & \text{if } f > f_c \end{cases} \tag{12}$$

where $d > 1$ is a coefficient representing the increased damaging effect of porosity after coalescence. Both f_c and d have to be adjusted. Failure occurs when $f_* = 1/q_1$.

In order to account for the plastic anisotropy of the material, the equivalent stress is that of the anisotropic yield function defined above. This modification of the GTN model is the same than the one used in Rivalin et al. (2001) [5]. It only affects the contribution of deviatory stresses on the potential definition. Damage is still assumed to be isotropic.

The plastic flow is obtained assuming normality so that the plastic strain rate tensor is given by:

$$\underline{\dot{e}}_p = (1-f)\dot{p}\frac{\partial f}{\partial \underline{s}} = (1-f)\dot{p}\frac{\partial s_*}{\partial \underline{s}} \tag{13}$$

The evolution of the damage variable is governed by mass conservation:

$$\dot{f} = (1-f)tr\underline{\dot{e}}_p \tag{14}$$

The parameters of this damage model are f_0, f_c et d. In this study, the initial porosity is set equal to the inclusions volume fraction determined by image analysis ($f_0 = 1.35 \times 10^{-4}$) in steel P. As discussed in Rivalin et al. (2001), Tanguy et al. (2005) [6] the mesh size in loading direction ($h_{load.}$) must also be considered as material parameter as it regulates crack growth. Thus three parameters were adjusted regarding experiments.

The mesh size used in the finite element simulation in loading direction of $200\mu m$ was found to work well for all tests specimens. The physically most important parameter is the critical void volume fraction, f_c, for which localization of plastic deformation and, hence, coalescence of voids occurs. The work of Benzerga et al (1999) [7] and Brocks et al (1995) [8] show that f_c generally depends on the triaxiality. In this study, f_c is adjusted to fit all tests with the loading direction in the T direction. Figure 9 shows the dependence of critical void volume fraction, f_c,

on the geometry (and then on the stress triaxiality) for the transverse loading direction in notched specimens. The range of triaxiality calculated from FE calculations are also indicated in figure 9.

The simulations were carried out for all specimen types with the loading direction in the T direction. The results are presented in figures 10 and 11. A good agreement between experiments and calculations in three point bending and CT specimens is obtained.

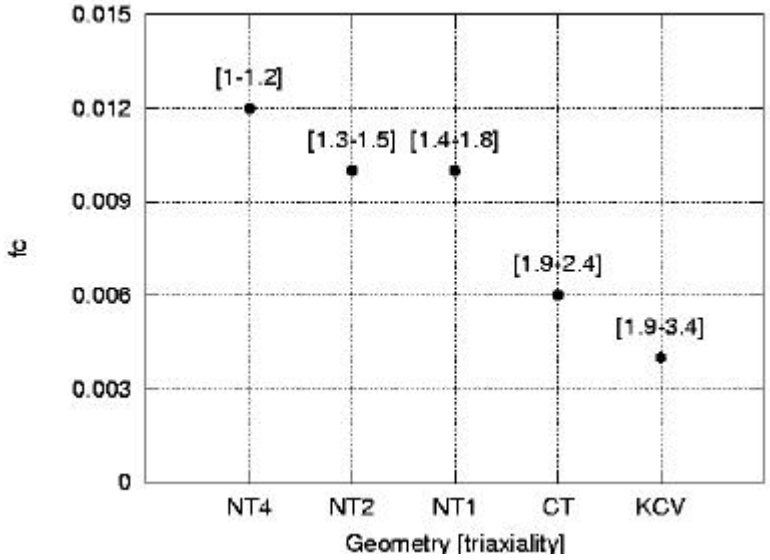

Figure 9: f_c - triaxiality curve for material X100 plate

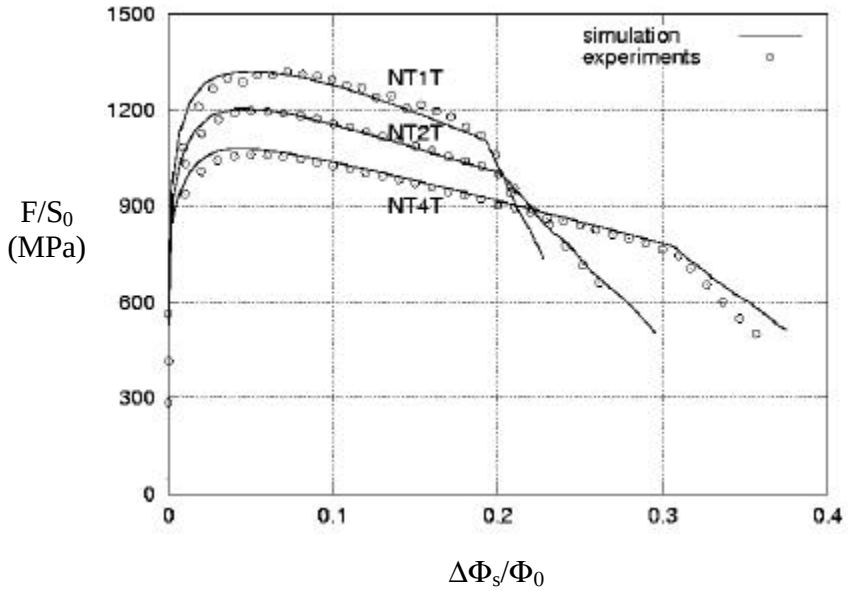

Figure 10: Simulations on notched samples for material X100 plate, loading is in T direction.

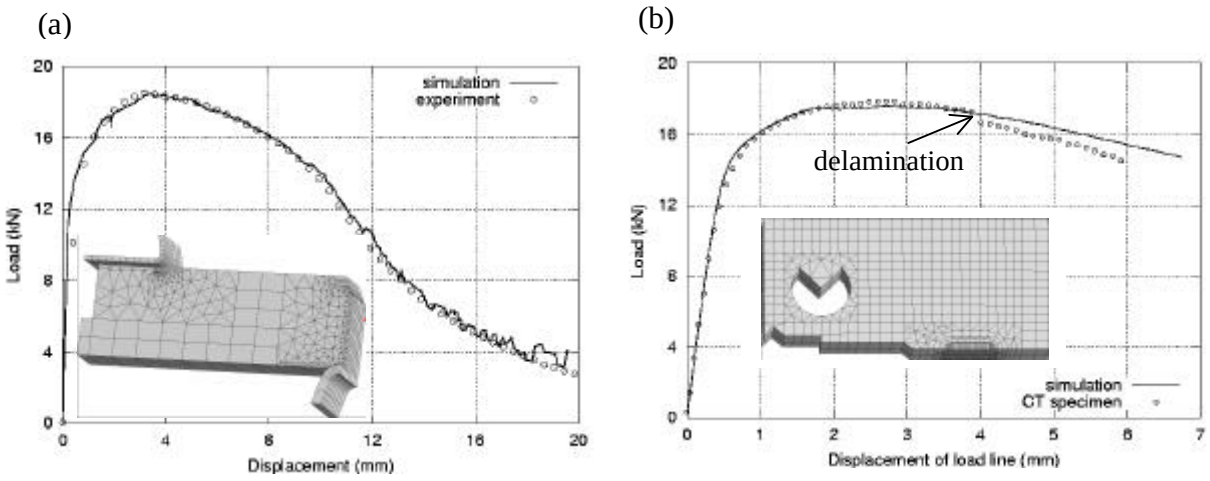

Figure 11: Simulations of (a) three point bending and (b) CT tests for material X100 plate material, loading is along T direction

Elastic properties	Young's modulus E	210GPa
	Poisson's ratio n	0.3
Plastic hardening	R_0, Q_1, k_1	580MPa, 0.367, 46.84
	Q_2, k_2	1.119, 0.741
Anisotropic model	a, a	9.25, 0.7
	c_1^1, c_2^1, c_3^1	1.022, 1.009, 0.961
	c_4^1, c_5^1, c_6^1	1.140, 1.116, 1.118
	c_1^2, c_2^2, c_3^2	1.572, 0.442, 0.536
	c_4^2, c_5^2, c_6^2	0.1, 0.924, 1.183
GTN model	q_1, q_2	1.5, 1
	f_0, d	$f_0 = 1.35\times10^{-4}$, 4.5
	f_c	see Fig. 9
Mesh size	$h_{load.}$, $h_{prop.}$, $h_{thick.}$	200, 280, 600-1200 mm

Table 4: Adjusted model parameters of the X100 steel plate

Conclusion

The behaviour of one of X100 linepipe steel was investigated using several specimen geometries: smooth tensile, notched tensile with different radii, compact tension. A unified constitutive equation was able to describe the elastoplastic and damage of this kind of steel. The compact tension and three point bending tests were then consistently simulated.

Acknowledgements

The authors wish to thank Jean-Pierre Jansen (EUROPIPE), Stéphane Hertz-Clémens (Gaz de France), Henri Godinot (TOTAL) as well as CEP&M (grant 6807/03) for active and financial support.

References

[1] Pineau, A. *Review of fracture micromechnisms and a local approach to predicting crack resistance in low strength steels*, ICF5, Vol. 2, 553-575, 1981.

[2] Palumbo, G., Tricarico, L., *J. Mater. Process. Technol.*, Vol. 164-165, 1089-1098, 2005

[3] Bron, F., Besson, J., *Int. J. Plas.*, Vol. 20, 937-963, 2004

[4] Tvergaard, V., Needleman, A., *Acta. Metall.*, Vol. 32, 157-169, 1984

[5] Rivalin, F., Besson, J., Di Fant, M., Pineau, A., *Eng. Fract. Mech.*, Vol. 68, 347-364, 2001

[6] Tanguy, B., Besson J., Piques, R., Pineau, A., ., *Eng. Fract. Mech.*, Vol. 72, 413-434, 2005

[7] Benzerga, A., Besson, J., Pineau, 1., *J. Eng. Mater. and Technol.*, Vol. 121, 221-229, 1999

[8] Brocks, W., Sun, D.-Z., Honig, A., *Int. J. Plas.*, Vol. 11, No. 8, 971-989, 1995